Atmospheric
Chemistry
and Physics

Discussions

# Aerosol radiative effects with dual view AOD retrievals

Stefan Kinne[1], Peter North[2], Kevin Pearson[2], Thomas Popp[3]

[1]MPI-Meteorology, Hamburg, Germany
[2]Swansea University, Swansea, Great Britain
[3]DLR, Pberpfaffenhofen, Germany

*Correspondence to*: Stefan Kinne (Stefan.Kinne@mpimet.mpg.de)

**Abstract.** Seasonal maps of dual view retrieved mid-visible AOD and AODf for four selected years (1998, 2008, 2019, 2020) are introduced and assessed in comparisons to MODIS retrievals and general data of an aerosol climatology. Due to different sensor capabilities (ATSR-2, AATSR and SLSTR) there are still unresolved inconsistencies so that decadal regional trends are not as detectable as with MODIS retrievals. SLSTR retrieval, however, agree with MODIS retrievals that 2020 Covid impacts on AOD values (via comparisons to the pre-COVID 2019 reference) are at best minor and secondary to natural anomalies by wildfires and dust. In radiative transfer applications the dual view AOD data for the four years are processed in the MAC climatology environment to determine aerosol associated radiative effects for total aerosol and for anthropogenic aerosol. Even though the calculated radiative effects are affected by retrieval AOD retrieval tendencies, climate relevant TOA net-flux changes are consistent to result with AOD data from other satellite sensors and a general climatology: -0.9W/m2 for total aerosol with a significant greenhouse effect and -0.8 and -0.2W/m2 for anthropogenic aerosol with and without indirect effects, respectively. Aside from global averages, seasonal maps highlight the diversity of regional and seasonal radiative effects.

## 1 Introduction

One decade ago, ESA's Aerosol Climate Change Initiative (CCI) set out to develop and improve retrievals for European satellite sensors. New products for aerosol properties were developed and user case studies were encouraged to demonstrate dataset usefulness for various applications, as part of the Aerosol_cci+ effort.

One such study here investigates aerosol associated radiative effects, by applying ESA's most advanced global aerosol datasets, which are based on the University of Swansea dual view retrievals for ATSR-2 [1997-2003], AATSR [2002-2012] and SLSTR [2017-2020]) satellite sensors with multi-spectral and dual (nadir and forward / rearward) viewing capabilities (*North et al. 2021, North 1999*). Four example years (1998, 2008, 2019 and 2020) were picked to address (1) temporal change by comparing 1998, 2008 and 2019 data and (2) potential COVID behavior impacts by comparing 2020 with 2019 data.

In the first part, seasonal averages of monthly gridded 1°x1° (latitude/longitude) level 3 aerosol optical depth (AOD) products for the four years are compared to same year MODIS sensor AOD retrievals (*Levy et al. 2013, Ginoux et al., 2012*) and to AOD data of the MAC aerosol climatology (*Kinne 2019*). MAC data are not associated with any specific year, but MAC captures general AOD expected patterns. In MAC, median AOD values from global aerosol component modeling with current emissions were forced to more realistic conditions by applying regional adjustments based on multi-annual monthly ground-based network AOD monitoring statistics (Aeronet). For a better understanding of maxima, decadal changes and differences are examined not only for total AOD but also fine-mode AOD (AODf). Hereby, AODf is the AOD contribution by (smaller) sub-micrometer size aerosol particles. These smaller sizes originate mainly from wildfires and pollution (thus also from anthropogenic sources) and by dominating aerosol number concentrations are particularly important for aerosol impacts on clouds.

39      In the second part, ATSR-2, AATSR and SLSTR monthly maps for AOD and AODf of all four years (1998,

40      2008, 2019 and 2020) are applied in an off-line radiative transfer environment to determine aerosol associated

41      radiative effects. In addition to effects by all aerosols also estimates for today's anthropogenic aerosol are provided –

42      without and with considering (first) indirect effects via aerosol modified water clouds. To illustrate spatial and

43      temporal variability impacts are presented in seasonal maps for radiative net flux changes (1) at the top of the

44      atmosphere (TOA), (2) at the surface and by their difference (3) for the atmosphere. Net flux changes at TOA

45      capture the climate impact (with a cooling indicated by negative changes and a warming indicated by positive

46      changes). Net flux reductions at the surface are relevant for surface exchange processes. And solar aerosol layer

47      heating of atmospheric impacts affect atmospheric dynamics (e.g. lifting/stabilizing aerosol layers).

48    **2 Dual view (DV) radiometer data**

49      The applied DV data are based on dual-view and multi-spectral SR heritage sensor retrievals by the

50      University of Swansea (*North et al., 2021*, *North 1999*). Gridded (1°x1° longitude/latitude) monthly level 3 data for

51      atmospheric aerosol column loads are examined for four different years: 1998 (ATSR-2), 2008 (AATSR), 2019

52      (SLSTR) and 2020 (SLSTR). The investigated aerosol properties are (1) the aerosol optical depth at 550nm (AOD)

53      and (2) the fine-mode aerosol optical depth at 550nm (AODf). AODf captures AOD contributions by sub-

54      micrometer size aerosols only.

55      For all four years (1998, 2008, 2019 and 2020) seasonal distribution maps and associated global averages

56      are compared for AOD and AODf in Figure 1.

57
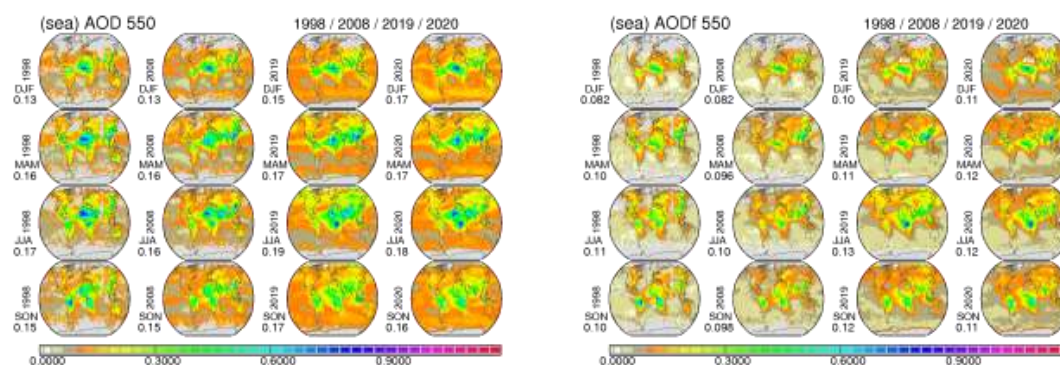


58
59
60 *Figure 1. Seasonal global distribution maps of retrievals for AOD (left panel) and AODf (right panel) with ATSR-2*
61 *1998 (col1), AATSR 2008 (col2), SLSTR 2019 (col3) and SLSTR 2020 (col4) data. Values to the lower left indicate*
62 *global seasonal averages.*
63

64      ATSR-2 and AATSR sensors have narrower swath widths compared to SLSTR sensors. In addition, the

65      SLSTR data presented here combine samples of two sensors on two different platforms. To compensate for poorer

66      statistics by ATSR-2 and AATSR retrievals, comparisons in Figure 1 are presented by season. All DV retrievals

67      generally agree on the major seasonal maxima. The maxima are related to wildfires over western Africa during DJF,

68      to dust over Sahara and Gobi deserts and pollution over SE Asia during MAM, to dust over (and off) the Sahara

69      desert, wildfires over central Africa and pollution over NH urban regions during JJA and to wildfires over southern

70    America and southern Africa during SON. We identify as remaining inconsistency that the annual global average

71    AOD and AODf values are about 15% larger for SLSTR compared to ATSR-2 and AATSR. While for all DV-

72    retrievals the fine-mode AOD fraction (AODf/AOD) for all is (relatively high at) near 65%, there are also consistent

73    differences with respect to the strength of maxima and of background. SLSTR retrievals yield larger AOD over

74    oceanic background and strongest wildfire maxima over the Congo during JJA, while ATSR-2 retrievals have

75    stronger dust maxima over the Sahara during dust seasons (MAM, JJA).

76          Regional and seasonal AOD and AODf differences are better visualized as differences to the same MAC

77    climatology (*Kinne, 2019a*) reference in Figure 2.

78
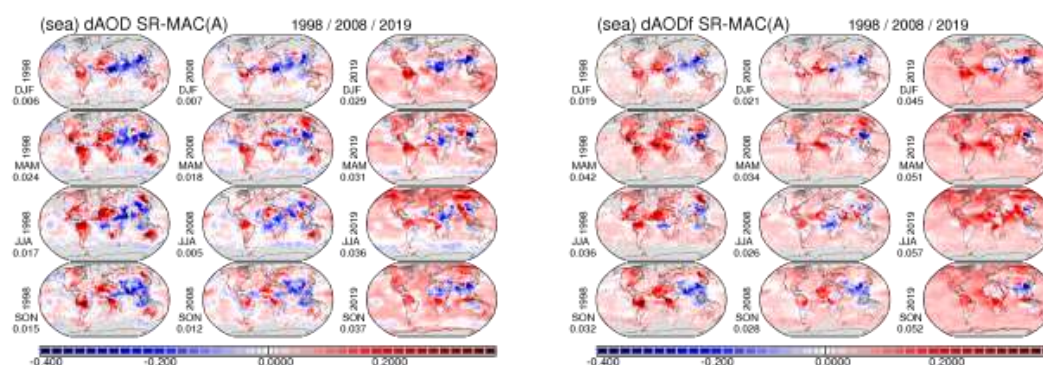


79
80
81    *Figure 2. Seasonal difference maps between DV retrievals for 1998 (col1), 2008 (col2) and 2019 (col3) and the*
82    *MAC climatology for AOD (left panel) and AODf (right panel). Values to the lower left indicate global seasonal*
83    *differences.*
84

85          Global averages of seasonal AOD are larger than for MAC - by about 15% for ATSR-2 and AATSR and by

86    about 30% for SLSTR. In addition, there are large regional differences, which vary in strength and even sometimes

87    in sign with DV sensor retrievals, which are in part caused by different sideways viewing strength and limitations

88    (SLSTR: forward, ATSR-2 and AATSR: rearward). Thus, attempts to derive decadal trends from DV retrievals are

89    not yet possible until DV sensor retrieval biases are better understood and corrected.

90          Deviations of concern to MAC and global modeling are the relatively high AODf attributions (also for dust

91    outflow across the Atlantic), higher wildfire AOD and lower AOD near the tropics from Africa to Asia in all DV

92    retrievals. Sensor specific larger deviations to MAC are for SLSTR retrievals the higher AOD background and

93    higher Northern hemisphere AOD (especially during JJA) and for ATSR-2 the higher AOD over the Sahara with

94    unexpected high fine mode contributions in ATSR-2.

95          In a different assessment, MODIS 6.1 Terra retrievals (*Levy et al., 2016 - over oceans, Ginoux et al, 2012 -*

96    *over land*) seasonal AOD and AODf data are compared for same available years (2008, 2019 and 2020) and

97    differences are presented in Figure 3.

98
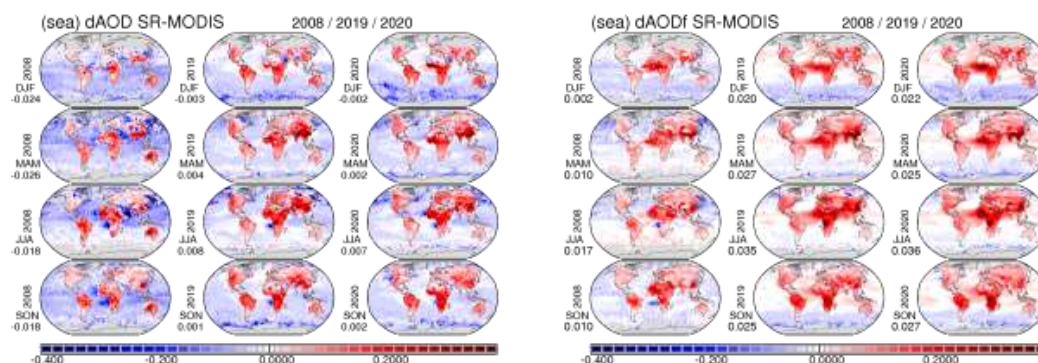
**Figure 3**: *Seasonal difference maps between DV retrievals and MODIS retrievals for 2008 (col1), 2019 (col2) and 2020 (col3) for AOD (left panel) and AODf (right panel). Values to the lower left indicate global seasonal differences.*

A first glance at Figure 3 reveals much lower DV AOD data over oceans and much higher AOD and AODf values over continents - in comparison to MODIS. While larger oceanic AOD by MODIS are likely in error due to contaminations by clouds (*Hyer et al. 2011*), the larger AOD values over land and the high fine mode AOD fraction of 65% (vs. about 50% in MODIS and MAC) are of concern in DV retrievals (note, that in DV and MODIS retrieval methods and assumptions differ over land and ocean).

## 3 AOD trends

DV retrievals from different sensors for selected years are not consistent enough (at this time) to address decadal trends. Twenty years (2001-2020) of MODIS retrievals (from the same sensor onboard one platform over the whole period), however, can offer information on recent trends for AODc (=AOD-AODf) and AODf. For information on semi-decadal trends monthly 1°x1° latitude/longitude AODc and AODf data of MODIS were binned into five year averages by season. Differences of the three 2006-2010, 2011-2015 and 2016-2020 averages to those of the 2001-2005 period are presented in Figure 4 (red colors indicate increases and blue colors decreases over time).
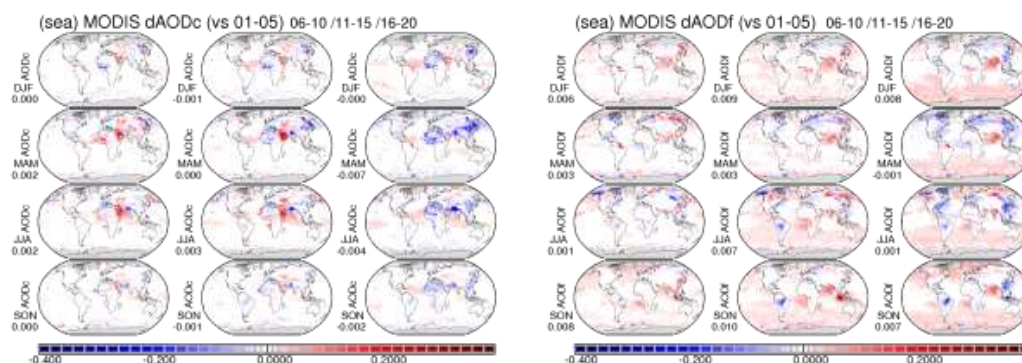


**Figure 4**: *Seasonal maps of semi-decadal trends for AODc (left panel) and AODf (right panel) based on MODIS retrievals. Lower left values indicate global seasonal trends.*

122

123     Semi-decadal changes for the total AOD and its AODc and AODf contributions since the year 2000 are

124     minor in terms of global averages. However, there are regional trends of both signs. For AODc, which mainly

125     reflects natural variability by mineral dust, there was more dust over Arabia between 2005-2015 (during MAM and

126     JJA), but less dust over northern India and eastern Asia (during MAM and JJA) and less dust over the Sahara since

127     2015. For AODf, which represents wildfire activities and pollution strength, less wildfires over southern America

128     since 2005 (during JJA and SON) but more wildfires over Siberia since 2010 (during JJA) occurred. Over urban

129     regions there are continuing pollution increases over India (outside the monsoon season), a strong reduction in

130     pollution though over eastern Asia since 2015 are continued reductions in pollution over the US and EU (during

131     MAM and JJA).


132     **4 COVID-19 impacts**

133     Same sensor SLSTR and MODIS retrievals for the years 2019 and 2020 were compared to explore potential

134     COVID impacts. Bi-monthly 2020 anomalies with respect to 2019 data for AOD, AODf and AODc differences are

135     presented in Figure 5.

136
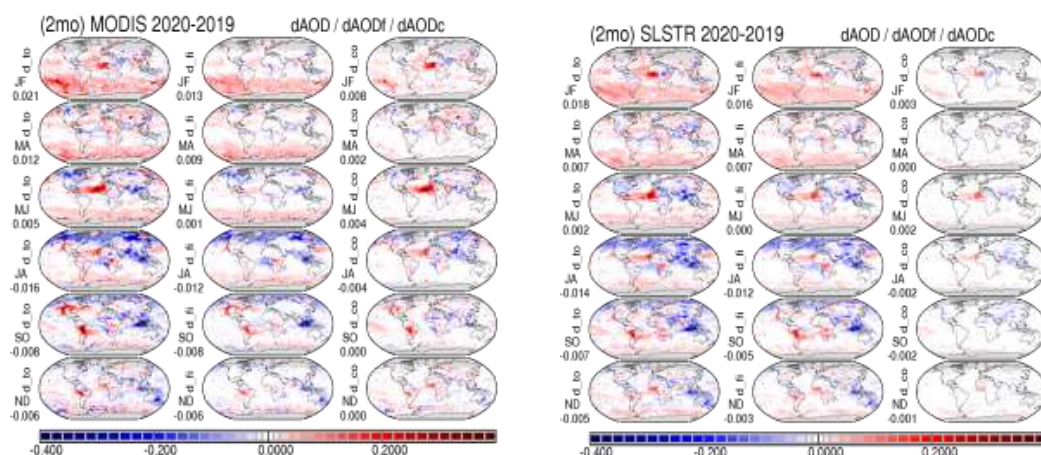


137
138     *Figure 5: Bi-monthly differences between 2020 and 2019 retrievals of MODIS (left panel) and SLSTR (right panel)*
139     *for AOD (col1), AODf (col2) and AODc (col3). Values to the lower left indicate 2-monthly global 2020-2019 anomaly*
140     *averages.*
141

142     During Covid-19 related shutdown periods (e.g. February and March 2020 over Eastern Asia, May and

143     April plus October to December 2020 over the U.S. and Europe), reduced traffic may have caused reductions in

144     AODf (and also in total AOD). However, when examining 2020-2019 AOD differences of both MODIS and SLSTR

145     in Figure 5, Covid-19 related reduced AOD signatures are difficult to find. Instead, for the 2-monthly (JF, MA, MJ,

146     JA, SO, ND) regional differences, specific (natural) events are the main modulators for differences.

147     -     Australian fires early in 2020 yielded positive AODf (and total AOD) anomalies over Southern

148           Hemispheric higher latitudes during JF and even for MA, as wildfire aerosol was partially convected (and

149           remained) in the stratosphere.

5

150   -   Boreal summer wildfires were stronger in 2019 for negative AODf (and total AOD) anomalies over

151       northern Canada during MJ and JA and over Siberia during JA.

152   -   Indonesian wildfires in the fall of 2019 caused negative AODf (and total AOD) anomalies over Indonesia

153       during JA and SO.

154   -   Wildfires over the Amazonas region were more intense during 2020 compared to 2019 and yielded positive

155       AODf (and total AOD) anomalies over Brazil during SO.

156   -   dust transport from the Sahara across the Atlantic were stronger in 2020 than in 2019 and caused positive

157       AODc (and total AOD) anomalies during MJ and JA.

158   In summary, Covid-19 impacts on atmospheric aerosol loads and aerosol associated climate impacts are at best

159   secondary - even on regional scales.

160   **6 Radiative transfer**

161   Simulations of atmospheric radiative transfer apply a two-stream radiative transfer model (*Kinne, 2019b*). In

162   that model, the spectral variability of atmospheric particle properties is represented by separate simulations in eight

163   solar and twelve infrared spectral sub-bands. In those 20 spectral bands, a total of 120 exponential terms are used to

164   represent atmospheric trace gas absorption. The daytime solar impact variability is covered by simulations at 9

165   different solar elevations. Atmospheric state and trace gas properties apply latitude and season relevant AFGL

166   (*Andersen et al., 1986*) standard atmospheres and the vertical variability is approximated by 20 plane-parallel

167   homogenous atmospheric layers. Land surface (visible and near-IR) albedo data of MODIS (*Schaaf et al., 2002*) are

168   applied, over open oceans a sun-elevation dependent albedo is considered (ref) and snow and ice coverage is based

169   on NOAA microwave data (*Taylor et al., 1996*). Cloud cover and cloud optical depth are represented by multi-

170   annual monthly ISCCP data (*Rossow et al., 1993*) and eight independent simulations cover all eight possible cloud

171   (high, mid, low) layer combinations. Simulations at each (of the 64800 1°x1° latitude/longitude) grid locations

172   averages for each month.

173   AOD and AODf monthly maps of ATSR-2, AATSR and SLSTR  replace those of the MAC aerosol

174   climatology (*Kinne, 2019a*). In the MAC climatology a monthly median AeroCom modeling background is

175   regionally and seasonally modified towards available monthly statistics by sun-/sky photometry of AERONET

176   (*Holben et al., 1999*) and MAN (*Smirnov et al, 2009*). Global modeling provides the needed information on aerosol

177   vertical distribution and on today's anthropogenic AODf fraction. For aerosol indirect effects by anthropogenic

178   aerosol a simple relationship from satellite retrievals over oceans linking cloud droplet number concentrations

179   (CDNC) and AODf is applied. This relationship translates anthropogenic AODf increases in reference to a (e.g. pre-

180   industrial) AODf background into CDNC increases. Associated decreases to the cloud droplet size (more but smaller

181   drops - assuming no changes to the cloud water content) define the (anthropogenic) aerosol associated aerosol

182   indirect effects.

183   Radiative impacts in the atmosphere are defined by differences of two simulations between a modified and

184   a standard configuration. All simulations consider ISCCP tropospheric clouds. These 'dual-call' radiative transfer

185   applications investigate

186

Atmospheric
Chemistry
and Physics
Discussions

187     -   *impacts of total aerosol presence (along with shortwave and longwave contributions)*

188     -   *impacts of anthropogenic aerosol presence (at TOA referred to as 'direct forcing')*

189     -   *impacts of reduced droplet radii by anthropogenic aerosol (at TOA: indirect forcing')*

190

191      Radiative forcing climate feedbacks (which cannot be considered in dual call simulations) are and can be

192 ignored, because long-term Earth System Model (ESM) simulations with fixed sea surface temperatures show that

193 atmospheric feedbacks may introduce forcing deviations of less than 10% (even smaller than AOD uncertainties for

194 total and especially pre-industrial AOD).

195      Anthropogenic aerosols are defined via a fraction of smaller sub-micrometer aerosol sizes (from global

196 modeling). Anthropogenic (land-use) contributions of dust are ignored, because (smaller size) dust radiative effects

197 are close to neutral. Also as only impacts of aerosols on lower altitude water clouds are allowed, only solar radiative

198 effects need to be considered for the impacts by anthropogenic aerosol.

199 **7 global radiative effects**

200      Aerosol radiative effects are determined separately for all four DV. Global averages of net fluxes at TOA

201 (negative: climate cooling, positive: climate warming) and at the surface (negative: loss, positive: gain) are summarized

202 in Table 1.

203
204 **Table 1** *Global annual averages for today's aerosol radiative effects at TOA and surface*
205

| | | TOA | | | | | | surface | | | | |
|---|---|---|---|---|---|---|---|---|---|---|---|---|
| | $W/m^2$ | ATSR2 | AATSR | SLSTR | SLSTR | *MAC* | | ATSR2 | AATSR | SLSTR | SLSTR | *MAC* |
| | | 1998 | 2008 | 2019 | 2020 | | | 1998 | 2008 | 2019 | 2020 | |
| total | sw+lw | - .87 | - .82 | - .95 | - .99 | *- .93* | | - 5.8 | - 5.6 | - 6.9 | - 6.9 | *- 4.6* |
| total | sw | - 1.5 | - 1.4 | - 1.5 | - 1.5 | *- 1.7* | | - 7.3 | - 7.1 | - 8.4 | - 8.4 | *- 6.4* |
| total | lw | + .66 | + .65 | + .60 | + .59 | *+ .76* | | + 1.5 | + 1.5 | + 1.4 | + 1.4 | *+ 1.8* |
| ant | direct | - .24 | - .24 | - .23 | - .22 | *- .23* | | - 2.1 | - 2.0 | - 2.6 | - 2.5 | *- 1.6* |
| ant | dir/ind | - .86 | - .86 | - .81 | - .80 | *- .89* | | - 2.7 | - 2.7 | - 3.2 | - 3.1 | *- 2.2* |

206

207      At TOA, today's total aerosol cools the climate by about -0.9W/m2. Hereby the stronger shortwave cooling

208 of about -1.5 W/m$^2$ is partially offset by about +0.6 W/m$^2$ of elevated (larger size) mineral dust. For anthropogenic

209 aerosol impacts, where smaller aerosol sizes contribute, mainly shortwave effects matter. The anthropogenic aerosol

210 via its added presence causes a climate cooling of about -0.2 W/m$^2$ and when effects by modified water clouds are

211 added, this climate cooling increases to about -0.8 W/m$^2$.

212      At the surface, today's aerosol reduces the radiative net flux much stronger than at TOA. Global average

213 surface net flux reductions of about -5.0 W/m$^2$ are composed of the shortwave losses of about -6.5 W/m$^2$ and

214 longwave gains of about +1.5 W/m$^2$, mainly due to elevated (larger size) mineral dust. The presence of

215 anthropogenic (added since pre-industrial times) aerosol reduces surface net fluxes by about -2.4 W/m$^2$, which is

216 further reduced to about -3.0 W/m$^2$, when impacts by aerosol modified clouds are included.

217    The radiative effects of aerosol in the atmosphere are captured by the difference of net flux impacts at TOA
218    and surface. Since reductions of net fluxes are larger at the surface than at TOA, the atmospheric impact is positive
219    which means an atmospheric heating. Global averages for atmospheric impacts are summarized in Table 2.
220
221    *Table 2 Global annual averages for today's aerosol solar atmospheric heating*
222

| | | total | | | | | anthropogenic | | | | |
|---|---|---|---|---|---|---|---|---|---|---|---|
| | *W/m2* | ATSR2 | AATSR | SLSTR | SLSTR | *MAC* | ATSR2 | AATSR | SLSTR | SLSTR | *MAC* |
| | | 1998 | 2008 | 2019 | 2020 | | 1998 | 2008 | 2019 | 2020 | |
| atm | sw+lw | + 4.9 | + 4.7 | + 6.0 | + 6.0 | *+ 3.7* | + 1.9 | + 1.8 | + 2.4 | + 2.3 | *+ 1.3* |

223

224    For the atmosphere, today's total aerosol heats the atmosphere on average by 5 $W/m^2$. Hereby, a 6 $W/m^2$
225    average solar heating is partially offset by an average 1 $W/m^2$ in infrared cooling. Atmospheric solar heating by
226    anthropogenic aerosol is about +2 $W/m^2$.
227    The global averages for the four DV retrieval years are similar at TOA to each other and even to standard
228    MAC simulations, which apply AOD and AODf maps of the MAC climatology. Since these MAC AOD values are
229    on average smaller than those of the DV retrievals, especially for SLSTR (as illustrated in Figure 2), SR retrieval
230    data associated global impacts are on average larger at the surface (and the atmosphere).


231    **7 other influential quantities**

232    To better understand aerosol radiative impacts, it is important to explain that aside from data for AOD
233    (and/or AODf) also other aerosol properties and several environmental properties are influential. Any such influence
234    would also need to be considered for the radiative forcing estimates, if any of those other quantities experienced a
235    trend during an observation period for AOD.
236    Important aerosol properties, other than AOD, are aerosol absorption strength, aerosol size and aerosol
237    altitude. Sensitivity calculations with the two-stream radiative transfer code show that if aerosol absorption
238    efficiency (i.e. 1-SSA) increases, then net flux losses at the surface are increased and at the same time TOA impacts
239    become less negative - both changes increase the inside atmosphere impacts. If aerosol includes contributions of
240    larger super-micrometer sizes (quantified by AODc), then interactions with longwave radiation cannot be ignored
241    anymore (in contrast to smaller wildfire and pollution aerosol). Longwave (and greenhouse / warming) effects
242    increase with aerosol absorption and aerosol elevation. Thus, elevated absorbing super-micrometer mineral dust can
243    yield significant longwave effects.
244    Important environmental properties are the incoming solar radiation, the solar elevation, the co-location
245    with clouds (and even with trace gases) and the surface radiative properties, such as solar albedo and temperature.
246    Every aerosol solar impact requires sunlight and the aerosol (back-) scattering is strongest near solar elevations of 20
247    degrees. Very important for TOA impacts is the co-location of aerosol with clouds. With clouds, aerosol (presence)
248    impacts are at most secondary - except for the case of absorbing aerosol above clouds: When aerosol dims the solar
249    reflection of clouds (to space), then the solar TOA impact of aerosols reverses to a warming. Similar to the 'aerosol
250    above cloud' scenario also an increasing brighter surface albedo reduces the potential for aerosols to cool to the point
251    that for (even weakly) absorbing aerosols over bright surfaces (e.g. snow) an aerosol TOA warming (by dimming)

252    the solar surface albedo can be expected. Surface temperature, temperature of the aerosol layer and trace gas

253    distributions only matter for super-micrometer size aerosols for longwave (greenhouse and re-radiation) effects.

## 8 seasonal and regional radiative effects

255         The global average impacts of Tables 1 and 2 are now brought to life in the subsequent presentation of

256    seasonal impact maps. With the average aerosol lifetime of a few days and with differences in solar insolation,

257    surface albedo and clouds, regional and seasonal impacts are highly diverse - sometimes even with changes to the

258    sign in the impact and with local absolute maxima up to an order of magnitude larger than global average values.

### 8.1 TOA net-flux impact distributions

260         Seasonal aerosol radiative effects at TOA associated with the four DV AOD retrievals for total aerosol

261    (presence) are presented in Figure 6, which also informs on shortwave and longwave contributions via annual

262    averages.

263
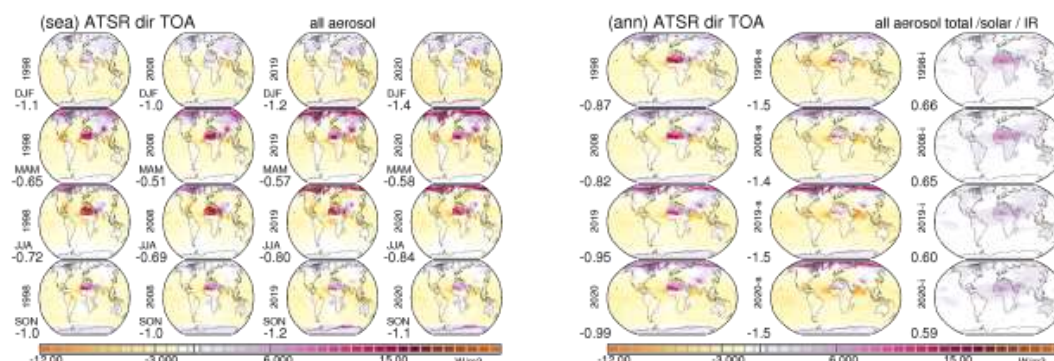


264
265
266    *Figure 6. Simulated total aerosol (presence) radiative effects at TOA with AOD data of ATSR-2 1998, AATSR 2008,*
267    *SLSTR 2019 and SLSTR 2020. Compared are seasonal impacts (left panel) and annual impacts (right panel), with*
268    *separations into its shortwave (-s) and longwave (-l) contributions. Positive values represent a warming and*
269    *negative values a cooling. Values to the lower left indicate global averages.*
270
271         Aerosol direct TOA radiative effects for total aerosol vary globally between - 0.8 and -1.2 W/m² (with the

272    stronger SLSTR cooling linked to its larger AOD). On a regional basis, TOA aerosol radiative effects vary between -

273    10 and +25 W/m², with the strongest cooling in dust outflow regions over oceans and the strongest warming over

274    (brighter) deserts. The solar effect is a cooling, except over brighter surfaces of deserts and especially snow/ice (of

275    polar regions). For elevated (even weakly) absorbing mineral dust the associated greenhouse effect contributes with a

276    significant warming, which is largely responsible for the peak warming over the Sahara.

277         Seasonal radiative effects by today's anthropogenic aerosol at TOA for the direct (aerosol presence) and the

278    combined direct and indirect effect are presented for the four DV AODf (and AOD) retrievals in Figure 7.

279
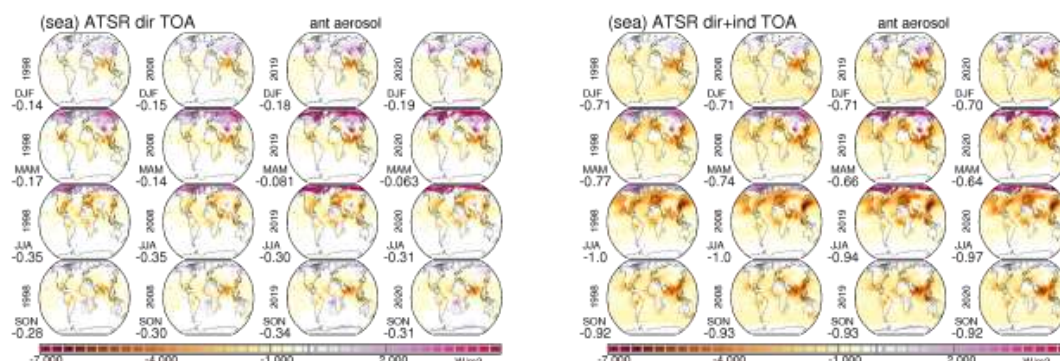
*Figure 7: Seasonal maps of simulated anthropogenic aerosol radiative effects at TOA with AODf data of ATSR-2 1998 (col1), AATSR 2008 (col2), SLSTR 2019 (col3) and SLSTR 2020 (col4). Positive values represent a warming and negative values a cooling. Direct (aerosol presence) impact maps (left panel) and combined direct and indirect (via modified clouds) impact maps (right panel) are presented. Values to the lower left are global seasonal averages.*

The direct aerosol (presence) forcing (TOA aerosol radiative effects at all-sky conditions) varies between -0.24 and -0.29 W/m$^2$, with the strongest cooling suggested by SLSTR and their larger AOD. Regionally and seasonally the aerosol direct forcing varies between -6.0 W/m$^2$ (pollution outflow offshore of urban regions during the summer) and +4.0 W/m$^2$ (absorbing aerosol over snow). The small warming during the SON season over the SE Atlantic is caused by the outflow of elevated absorbing wildfire aerosol as it dims the solar albedo of lower stratocumulus cloud fields. Overall regions with climate cooling dominate.

The combined direct and indirect (considering aerosol induced reductions to the droplet size of water clouds) aerosol forcing is almost identical at -0.87 W/m$^2$. Regionally and seasonally, the combined anthropogenic forcing varies between -6.0 and +2.0 W/m$^2$. Compared to direct forcing the climate cooling over urban regions and over (dark) oceanic regions with pollution outflow is increased. Also, the direct SON dimming over the Southeast Atlantic is gone. The JJA season contributes with the strongest cooling.

## 8.2 surface net-flux impact distributions

Seasonal aerosol radiative effects at the surface associated with the four DV AOD retrievals for total aerosol (presence) are presented in Figure 8, which also informs on shortwave and longwave contributions via annual averages.

Aerosol direct radiative effects for total aerosol at the surface vary globally between -5.4 and -6.4 W/m$^2$ (with the stronger SLSTR cooling linked to its larger AOD). On a regional basis the surface aerosol radiative effects vary between -40 and 0 W/m$^2$. The strongest cooling occurs near continental aerosol source regions, especially if large AOD data combine with a strong aerosol absorption potential (of wildfires and urban pollution). Aside from reductions to the solar radiation there are also IR re-radiation gains by elevated (colder) dust, so that for mineral dust impacts reductions of solar net fluxes at the desert surface are almost compensated by infrared net flux gains.

Atmospheric
Chemistry
and Physics
Discussions
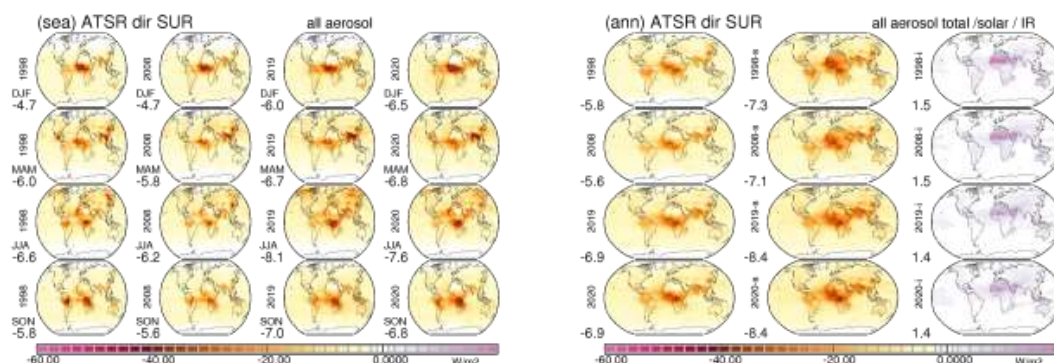


**Figure 8.** *Simulated total aerosol (presence) radiative effects at the surface with AOD data of ATSR-2 1998, AATSR 2008, SLSTR 2019 and SLSTR 2020. Compared are seasonal impacts (left panel) and annual averages (right panel) with separations into its shortwave (-s) and longwave (-l) contributions. Positive values represent surface net-flux gains and negative values surface net-flux losses. Values indicate global averages.*

Seasonal aerosol radiative effects by today's anthropogenic aerosol at the surface for the direct (aerosol presence) and for the combined direct and indirect effect are presented for the four DV AODf retrievals in Figure 9.
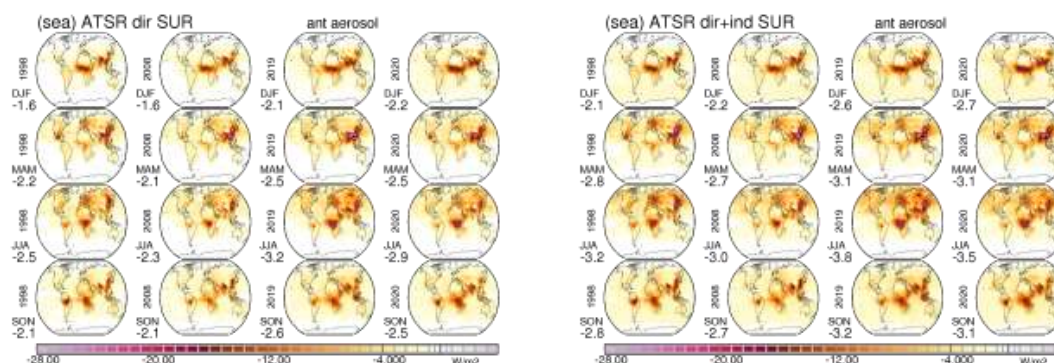


**Figure 9**. *Seasonal maps of simulated anthropogenic aerosol radiative effects at the surface with AODf data of ATSR-2 1998 (col1), AATSR 2008 (col2), SLSTR 2019 (col3) and SLSTR 2020 (col4). There are only negative values which represent net flux losses at the surface. Direct (aerosol presence) impact maps (left panel) and combined direct and indirect (via modified clouds) impact maps (right panel) are presented. Values to the lower left are global seasonal averages.*

The direct radiative effects by anthropogenic aerosol at the surface vary globally between -1.5 and -1.9 W/m$^2$, with stronger SLSTR net flux reduction linked to its larger AOD. All surface radiative effects are only negative and can be as large as -20 W/m$^2$. The strongest cooling occurs over continental regions and seasons with (strongly absorbing) wildfire and (absorbing) urban pollution. Maximum solar net flux reductions are over Eastern Asia during MAM and for SLSTR data over the Congo regions during JJA.

The combined direct and indirect radiative effects by anthropogenic aerosol at the surface vary globally between -2.6 and -3.1 W/m$^2$ with stronger SLSTR net flux reduction linked to its larger AOD. All surface radiative

334    effects are negative and slightly more negative than the direct effect. Compared to the direct impact, net flux

335    reductions at the surface are mainly increased over (dark) ocean regions affected by pollution outflow.

336    **8.2 atmospheric net-flux impact distributions**

337    Seasonal aerosol radiative effects in the atmosphere for total and anthropogenic aerosol are presented for the

338    four DV AOD and AODf retrievals in Figure 10.

339
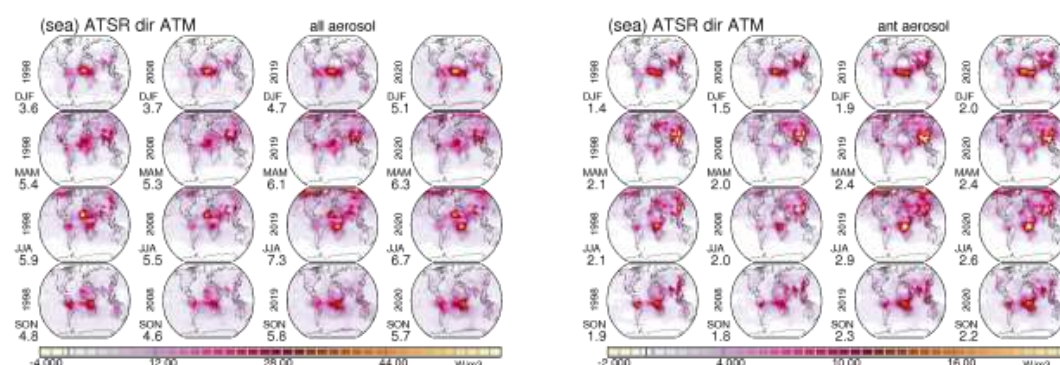


340
341
342    *Figure 10: Seasonal maps of simulated aerosol radiative impacts on the atmosphere with AOD and AODf data of*
343    *ATSR-2 1998 (col1), AATSR 2008 (col2), SLSTR 2019 (col3) and SLSTR 2020 (col4). Positive values by shortwave*
344    *heating dominate. Atmospheric impacts are presented for total (left panel) and anthropogenic aerosol (right panel).*
345    *Values to the lower left indicate global seasonal averages.*
346

347    The direct radiative effect in the atmosphere varies globally for total aerosol between +4.5 and +5.7 W/m$^2$

348    and for anthropogenic aerosol between +1.7 and +2.2 W/m$^2$. The stronger atmospheric heating with SLSTR data is

349    due to its larger AOD. The aerosol atmospheric effects are positive and can reach above +30 W/m$^2$ over regions with

350    strong aerosol absorption values. The strongest solar heating is over the biomass burning regions of western Africa in

351    the DJF season and over the Congo region in the JJA season.

352    **9 discussions**

353    The strengths of simulated aerosol radiative impacts are certainly modulated by the aerosol optical depth

354    maps used, as demonstrated by the larger SLSTR impacts with their larger AOD (compared to ATSR-2, AATSR and

355    MAC). For more accurate impact estimates more accurate and more consistent satellite data (also to other sensor

356    retrievals for the same period) in terms of distributions and maxima are required. Another aspect, especially for the

357    accuracy of anthropogenic impacts, is the AOD attribution to smaller aerosol sizes. The DV retrievals have a

358    AODf/AOD ratio, which is much larger than in MODIS retrievals or global modeling. In general, higher AODf

359    values yield stronger anthropogenic direct effects but weaker indirect effects - via a higher pre-industrial reference

360    background. Despite open issues in DV retrievals for AOD and AODf, the regional and seasonal aerosol radiative

361    effects maps offer systematic insights and context to (single value) global averages.

362

363

364

**10 summary**

366       A user case study first examined and then applied (in a radiative transfer study) monthly 1°x1°
latitude/longitude gridded mid-visible AOD and AODf data based on dual view (DV) retrievals for four selected
years: 1998 with the ATSR-2 sensor, 2008 with the AATSR sensor and 2019 and 2020 with SLSTR sensors from
two different platforms. DV-retrieved AOD maps differed mainly due to different sensor capabilities with higher
oceanic background and higher NH continental summer values in SLSTR. While any extraction of decadal change
by comparing 1998, 2008 and 2019 DV data is  discouraged, long term changes for AOD, AODc and AODf between
2001 and 2020 are offered by consistently retrieved MODIS sensor data. Even in comparisons of five year averages,
variability of major natural aerosol events dominate. Still, with respect to anthropogenic change, AODf changes over
urban regions document (1) continued pollution increase over (northern) India outside the Monsson season, (2)
strong reductions over eastern Asia since 2015 and (3) ongoing reductions in pollution over the U.S. and EU (during
MAM and JJA). Comparing 2020 with 2019 data, signals of Covid-19 related reductions of AODf (due to reduced
industrial activities and traffic) were ay best secondary to natural anomalies both with SLSTR and MODIS data.

378       In an application, the DV AOD and AODf maps for the four selected years were applied in radiative
transfer simulations to determine associated aerosol radiative effects for total aerosol and for today's anthropogenic
aerosol. The calculated radiative effects for all four years are similar, with larger effects usually associated with the
higher AOD in SLSTR (over oceans and most continental regions) compared to ATSR-2 and AATSR. At TOA,
though, global average impacts with AOD and AODf maps for all four years were similar with a -0.9 W/m$^2$ cooling
for total aerosol and a -0.8 W/m$^2$ climate cooling for anthropogenic aerosol - including a -0.6 W/m$^2$ cooling by (first)
indirect effects through clouds.

385       For radiative impacts of total aerosol it is also demonstrated that with the presence of elevated mineral dust
longwave radiative impacts must be included, hereby offsetting on a global average about 20% of the solar impacts.
Seasonal impact maps are offered to detail the highly diverse seasonal and regional nature of aerosol radiative
effects, which are often a magnitude larger than their associated global averages and at TOA, radiative effects even
can switch their sign.

**10 acknowledgements**

394

395

Atmospheric
Chemistry
and Physics
Discussions

**References**

Anderson, G., Clough, S., Kneizys, F., Chetwynd. J. and Shettle, E.: AFGL Atmospheric Constituent Profiles
(0.120km) Air Force Geophysics Lab, Hanscom AFB, MA, 1986.

Ginoux, P., Prospero, J., Gill, E., Hsu, C., and Zhao, M.: Global scale attribution of anthropogenic and natural dust
sources and their emission rates based on MODIS deep blue aerosol products, Rev. Geophys., 50, RG3005,
2012.

Holben, B., et al. An emerging ground-based aerosol climatology: Aerosol Optical Depth from AERONET, J.
Geophys. Res., 106, 12067-12097, 1999.

Hyer, E. J., J. S. Reid, and J. Zhang, An over-land aerosol optical depth data set for data assimilation by filtering,
correction, and aggregation of MODIS Collection 5 optical depth retrievals, Atmospheric Measurement
Techniques, 4, 379-408, 2011.

Kinne S., The MACv2 aerosol climatology, Tellus B chemical and physical Meteorology, 71, 1-21, 2019a.

Kinne, S., Aerosol radiative effects with MACv2, Atmos. Chem. Phys.19 10919-10958, 2019b.

Levy R., Matteo, S., Muchack, L., Remer, L., Sayer, A., Patadia, F. and Hsu, C.: The collection 6 MODIS aerosol
products over land and ocean. Atmos. Meas. Techn. 6 (11), 2013.

North, P., Heckel, A. and Pearson, K.: SU-SLSTR ATBD, CS3, Copernicus Climate Data store
(cds.climate.copernicus.eu), 2021.

North, P., Estimation of aerosol opacity and land surface bi-directional reflectance from ATSR-2 dual angle imagery.
J.Geophys. Res., Atmos 107 (D12), 1-10, 1999.

Rossow, W., Walker, A., and Garder, C.: Comparison of ISCCP and other cloud amounts, J. Climate, 6, 2394-2418,
1993.

Schaaf, C., Gao, F., Strahler, A., Lucht, W., Li, X., Trang, T., Strucknell, N., Zhang, X., Jin, Y., Mueller, J., Lewis,
P., Barnsley, M., Hobson, P., Disney, M., Roberts, G., Dunderdale, M., D'Entremont, R., Hu, B., Liang,
S.,Privette, J. and Roy, D.: First observational BRDF, albedo and nadir reflectance from MODIS, Remote
Sens. Environ. 83, 135-148, 2002.

Smirnov, A., et al.: Maritime Aerosol Network as a component of Aerosol Robotic Network, *J.Geophys. Res.*, 114**,**
D06204, 2009.

Taylor, J., Edwards, J., Glew, M., Hignett, P. and Slingo, A.: Studies with a flexible new radiation code. II:
Comparisons with aircraft shortwave observations, Q. J. Roy. Meteor. Soc. 122, 839– 861, 1996.